NASA/TM—2002–211604

Sensitivity of Global Sea-Air CO_2 Flux to Gas Transfer Algorithms, Climatological Wind Speeds, and Variability of Sea Surface Temperature and Salinity

S.R. Signorini and C.R. McClain

National Aeronautics and
Space Administration

Goddard Space Flight Center
Greenbelt, Maryland 20771

April 2002

The NASA STI Program Office ... in Profile

Since its founding, NASA has been dedicated to the advancement of aeronautics and space science. The NASA Scientific and Technical Information (STI) Program Office plays a key part in helping NASA maintain this important role.

The NASA STI Program Office is operated by Langley Research Center, the lead center for NASA's scientific and technical information. The NASA STI Program Office provides access to the NASA STI Database, the largest collection of aeronautical and space science STI in the world. The Program Office is also NASA's institutional mechanism for disseminating the results of its research and development activities. These results are published by NASA in the NASA STI Report Series, which includes the following report types:

- TECHNICAL PUBLICATION. Reports of completed research or a major significant phase of research that present the results of NASA programs and include extensive data or theoretical analysis. Includes compilations of significant scientific and technical data and information deemed to be of continuing reference value. NASA's counterpart of peer-reviewed formal professional papers but has less stringent limitations on manuscript length and extent of graphic presentations.
- TECHNICAL MEMORANDUM. Scientific and technical findings that are preliminary or of specialized interest, e.g., quick release reports, working papers, and bibliographies that contain minimal annotation. Does not contain extensive analysis.
- CONTRACTOR REPORT. Scientific and technical findings by NASA-sponsored contractors and grantees.
- CONFERENCE PUBLICATION. Collected papers from scientific and technical conferences, symposia, seminars, or other meetings sponsored or cosponsored by NASA.
- SPECIAL PUBLICATION. Scientific, technical, or historical information from NASA programs, projects, and mission, often concerned with subjects having substantial public interest.
- TECHNICAL TRANSLATION. English-language translations of foreign scientific and technical material pertinent to NASA's mission.

Specialized services that complement the STI Program Office's diverse offerings include creating custom thesauri, building customized databases, organizing and publishing research results . . . even providing videos.

For more information about the NASA STI Program Office, see the following:

- Access the NASA STI Program Home Page at http://www.sti.nasa.gov/STI-homepage.html
- E-mail your question via the Internet to help@sti.nasa.gov
- Fax your question to the NASA Access Help Desk at (301) 621-0134
- Telephone the NASA Access Help Desk at (301) 621-0390
- Write to:
  NASA Access Help Desk
  NASA Center for AeroSpace Information
  7121 Standard Drive
  Hanover, MD 21076-1320

NASA/TM—2002–211604

Sensitivity of Global Sea-Air CO_2 Flux to Gas Transfer Algorithms, Climatological Wind Speeds, and Variability of Sea Surface Temperature and Salinity

Charles R. McClain, NASA Goddard Space Flight Center, Greenbelt, Maryland
Sergio Signorini, SAIC, Beltsville, Maryland

National Aeronautics and
Space Administration

Goddard Space Flight Center
Greenbelt, Maryland 20771

April 2002

Available from:

NASA Center for AeroSpace Information
7121 Standard Drive
Hanover, MD 21076-1320
Price Code: A17

National Technical Information Service
5285 Port Royal Road
Springfield, VA 22161
Price Code: A10

PROLOGUE

Sensitivity analyses of sea-air CO_2 flux to gas transfer algorithms, climatological wind speeds, sea surface temperature (SST) and salinity (SSS) were conducted for the global oceans and selected regional domains. Large uncertainties in the global sea-air flux estimates are identified due to different gas transfer algorithms, global climatological wind speeds, and seasonal SST and SSS data. The global sea-air flux ranges from -0.57 to -2.27 Gt/yr, depending on the combination of gas transfer algorithm and climatological wind speeds used. Different combinations of SST and SSS global fields resulted in changes as large as 35% on the oceans global sea-air flux. An error as small as ±0.2 in SSS translates into a ±43% deviation on the mean global CO_2 flux. This result emphasizes the need for highly accurate satellite SSS observations for the development of remote sensing sea-air flux algorithms.

There are significant regional patterns in the distribution of oceanic sources and sinks of CO_2. The Southern Ocean (-0.58 to -1.48 Gt/yr), North Atlantic (-0.27 to -0.73 Gt/yr), and North Pacific (-0.17 to -0.48 Gt/yr) are the largest sinks of CO_2 throughout the year. The equatorial Pacific is the largest source of CO_2 (0.28 to 0.81 Gt/yr) with positive values throughout the year. The Indian Ocean and the equatorial Atlantic are weak sources of CO_2 throughout the year (0.04 to 0.16 Gt/yr). The Southern Ocean has the largest seasonal cycle with a peak in ocean uptake during January-February (-1.10 to -2.86 Gt/yr). The North Atlantic and North Pacific Oceans have a reduced seasonal cycle, with strongest uptake during fall-winter and nearly neutral conditions during the summer months. These regions have small outgassing (North Pacific) or small ingassing (North Atlantic) of CO_2 during the summer months because the potentially high pCO_2 values due to elevated SST conditions are counterbalanced by an increased pCO_2 drawdown by biological activity. The Indian Ocean, equatorial Pacific, and equatorial Atlantic have no distinctive seasonal cycle.

TABLE OF CONTENTS

1. Introduction

The global sea-air flux of CO_2 is strongly dependent on the sea-air pCO_2 difference (ΔpCO_2) and the gas exchange coefficient. These two components of the air-sea flux have similar ranges of variability in the ocean and, therefore, are equally important in determining the accuracy of the estimated flux. The gas exchange coefficient is primarily a function of the wind speed (Liss and Merlivat, 1986; Tans *et al.*, 1990; Wanninkhof, 1992), but the ocean pCO_2 is highly dependent on temperature and salinity, which is a primary focus of this study. The ocean pCO_2 is a function of the total carbon dioxide TCO_2 concentration, the total alkalinity (Lee *et al.*, 2000), and dissociation constants for the chemical components of the CO_2 system (Antoine and Morel, 1995; Signorini *et al.*, 2001a; Signorini *et al.*, 2001b). The dissociation constants are functions of temperature and salinity (Dickson and Millero, 1987). The distribution of surface alkalinity in the open ocean is mainly controlled by the factors that govern salinity (Broecker and Peng, 1982; Millero *et al.*, 1998). Therefore, accurate measurements of seasonal and interannual changes of surface salinity and temperature of the world's oceans is central to studies of global carbon flux. The biological uptake of CO_2 is also an important component of the carbon cycle in the oceans. Algorithms for primary production that rely on satellite ocean color data (Behrenfeld *et al.*, 2001) provide an important tool for global assessments of biological effects on the pCO_2 variability.

Traditional methods (hydrographic cruises) of salinity and temperature measurements have been used for many years to compile comprehensive climatological data sets (Conkright *et al.*, 1998). More recent studies, for example, the World Ocean Circulation Experiment (WOCE), have amplified our knowledge of the salinity and temperature variability in the oceans. The use of remote sensing techniques, e.g., AVHRR for sea surface temperature (SST), combined with optimal interpolation using ancillary *in situ* data (Reynolds and Smith, 1994), provides much higher spatial and temporal resolution of the SST of the world's oceans. More recently, remote sensing of sea surface salinity (SSS) has become a viable technique (Lagerloef *et al.*, 1995) and efforts are currently underway at NASA and the European Space Agency (ESA) to design satellite salinity sensors. Should global remote sensing of SSS with sufficient accuracy become operational, the data would be invaluable for estimating global carbon fluxes. In this NASA Technical Memorandum, we conduct a sensitivity analysis of the global sea-air CO_2 flux to gas transfer algorithms, climatological wind speeds, and variability of surface salinity and temperature.

2. Methodology and Data Sources

We used an ocean pCO_2 model (Signorini *et al.*, 2001a; Signorini *et al.*, 2001b), combined with algorithms for TA and gas transfer, to estimate the seasonal sea-air CO_2 flux for the global oceans. The required input data for the ocean pCO_2 model are SST, SSS, TA, and TCO_2. The seasonal TA was obtained from the algorithm of Millero *et al.* (1998), which is a function of SST and SSS,

$$TA = NTA\frac{SSS}{35} \qquad (1)$$

$$\mathrm{NTA}=A+B(\mathrm{SST}-T_o)+C(\mathrm{SST}-T_o)^2 \qquad (2)$$

where NTA is the normalized TA. The coefficients A, B, and C, and reference temperature T_o, vary according to specific ocean basins and regional domains (Millero *et al.*, 1998). The seasonal SST and SSS global fields are from the World Atlas 1998 (Conkright *et al.*, 1998). For the purposes of this analysis the TA estimates are assumed to be error-free.

Existing TCO_2 algorithms are still not accurate enough to retrieve required ΔpCO_2 values within reasonable limits. Over the global oceans, ΔpCO_2 vary from -100 µatm to +100 µatm, but its global mean is always between 0 and -6 µatm. An error of 1 µmol/kg in TCO_2 translates into an error of ~1.5 µatm on pCO_2. Lee *et al.* (2000) compared TCO_2 fields obtained with their SST and SSS algorithm to the TCO_2 fields obtained from the combination of Takahashi *et al.* (1997) pCO_2 data and TA fields. The differences are very large (±40 µmol/kg). For this reason we computed the TCO_2 seasonal fields from available ocean pCO_2 data (Takahashi *et al.*, 1997), seasonal TA fields derived from the Millero *et al.* (1998) algorithm, and SST and SSS from World Atlas 1998 (Conkright *et al.*, 1998) climatology. Therefore, the TCO_2 seasonal fields calculated this way, combined with the TA, SST, and SSS seasonal fields, reproduce the seasonal pCO_2 data from Takahashi *et al.* (1997) exactly. The combination of these input data sets was used to perform the sensitivity analysis in this study.

The air-sea CO_2 flux (FCO_2) is calculated using the following formulation:

$$FCO_2 = \rho K_o \alpha \Delta pCO_2 \qquad (3)$$

where ρ is the water density (kg m^{-3}), K_o is the gas transfer coefficient, ΔpCO_2 (µatm) is the difference between sea and air pCO_2, and α is the CO_2 solubility (mol kg^{-1} atm^{-1}), which is calculated from temperature (°K) and salinity using the formulation of Weiss and Price (1980),

$$\ln\alpha = -162.8301 + 218.2968\ln\left(\frac{100}{T_K}\right) + 90.9241\left(\frac{T_K}{100}\right) - 1.47696\left(\frac{T_K}{100}\right)^2 + S\left[0.025695 - 0.025225\left(\frac{T_K}{100}\right) + 0.0049867\left(\frac{T_K}{100}\right)^2\right] \qquad (4)$$

Four gas transfer algorithms were used. The algorithms are a function of the wind speed u in m s^{-1}:

I. Liss and Merlivat (1986):

$$\begin{aligned} k_w &= 0.17u && \text{, for } u \le 3.6 \\ k_w &= 2.85u - 9.65 && \text{, for } 3.6 < u \le 13 \\ k_w &= 5.9u - 49.3 && \text{, for } u > 13 \end{aligned} \tag{5}$$

II. Wanninkhof (1992) for long-term averaged wind:

$$k_w = 0.31\,u^2 \tag{6}$$

III. Tans *et al.* (1990) for $u > 3$ m s^{-1} (E=0 for $u < 3$ m s^{-1}):

$$E(\text{moles } CO_2 \text{ m}^{-2}\text{year}^{-1}\mu\text{atm}^{-1}) = 0.016[u-3] \tag{7}$$

IV. Wanninkhof and McGillis (1999) for long-term averaged wind:

$$k_w = 1.09u - 0.333u^2 + 0.078u^3 \tag{8}$$

For algorithms I, II, and IV, equation (3) is used with K_o (cm h^{-1}) defined as

$$K_o = k_w\left(\frac{Sc}{660}\right)^{-\frac{1}{2}} \tag{9}$$

where Sc is the Schmidt number given by

$$Sc = 2073.1 - 125.62\text{SST} + 3.6276\text{SST}^2 - 0.043219\text{SST}^3 \tag{10}$$

For the Tans *et al.* (1990) algorithm (III), FCO_2=E ΔpCO_2 in units of moles CO_2 m^{-2} year^{-1}. To convert FCO_2 to moles CO_2 m^{-2} year^{-1} in equation (3), we must convert K_o to m yr^{-1} (K_o $\times$24$\times$365/100) and α to mol kg^{-1} μatm^{-1} ($\alpha\times10^{-6}$).

The atmospheric surface pCO_2 data was obtained from the NOAA/GMCC Flask Sampling Network (Conway and Tans, 1996). These data are available from numerous sites on the globe, with the longest record covering the period of 1967-1993. The secular trend of atmospheric CO_2 does not change significantly throughout the Earth's atmosphere, but the seasonal cycle does. The amplitude of the seasonal cycle is largest at high northern latitudes and smallest at the south pole due to the geographic distribution of land vegetation and marine phytoplankton affecting the spring-summer uptake of CO_2 via photosynthesis. Seasonal global distribution of atmospheric pCO_2 for 1990 was obtained from concurrently available data at three sampling sites, Cold Bay (55°N), Mauna Loa (19.5°N), and the south pole (90°S). The year 1990 was chosen because it is

the reference year used by Takahashi *et al.* (1997) to correct the pCO_2 observations used in their global carbon flux estimates. Therefore, our carbon flux estimates are also for 1990.
Seasonal averages were obtained from 3-month composites coinciding with the SST and SSS seasonal averages. A latitude-dependent global seasonal distribution of atmospheric pCO_2 at one-degree resolution was constructed by spline interpolation (Akima, 1970) based on the three concurrently available records from the three chosen sites (Figure 1).

Each of the four algorithms were used with three different wind speed climatologies: Esbensen and Kushnir (1981), wind scatterometer data from European Remote Sensing (ERS) Satellites, and winds (Wentz, 1997) derived from the Special Sensor Microwave/ Imager (SSM/I). The ERS (www.ifremer.fr/cersat/), SSM/I (www.ssmi.com), and Esbensen&Kushnir (ingrid.ldeo.columbia.edu) winds were obtained via the web. The seasonal wind speed maps for these three climatological data sets are shown in Figures 2, 3, and 4, respectively.

Sensitivity tests were also conducted with different SST and SSS climatologies. These included the World Ocean Atlas 1998 (Conkright *et al.*, 1998), the World Ocean Atlas 1994 (Levitus and Boyer, 1994; Levitus *et al.*, 1994), and the Reynolds and Smith SST data (Reynolds and Smith, 1994).

3. Sensitivity to Gas Transfer Algorithms and Wind Speed Climatologies

Results from the application of the three wind speed climatologies and four different gas transfer algorithms are provided for the global oceans and regional domains in Tables 1, 2, and 3, and in Figures 5 through 10. Figures 5, 6, and 7 show the seasonal and spatial variability of the sea-air CO_2 flux for the four gas transfer algorithms and the three different wind speed climatologies. A summary of globally and regionally averaged wind speeds for the three wind data sets is provided in Table 4. The sea-air flux varies with the gas transfer algorithm and wind speed climatology used. As summarized in Tables 1, 2, and 3, the smallest global sea-air CO_2 flux is obtained with the Liss and Merlivat (1986) gas transfer algorithm for all three wind speed climatologies. The SSM/I winds (Table 2) produce the lowest global flux (-0.57 Gt/yr), while the ERS winds (Table 3) produce the highest flux (-0.70 Gt/yr). As shown in Table 1, the winds from Esbensen and Kushnir (1981) yield a global sea-air flux (-0.65 Gt/yr) between the ERS and SSM/I results. A negative sea-air flux represents uptake of CO_2 by the ocean. The largest global sea-air CO_2 flux is obtained with the Wanninkhof and McGillis (1999) gas transfer algorithm. This algorithm yields yearly global sea-air CO_2 fluxes of -2.27, -2.01, and -1.73 Gt/yr using the ERS, Esbensen and Kushnir (1981), and SSM/I wind climatologies, respectively. The Southern Ocean (-0.58 to -1.48 Gt/yr), North Atlantic (-0.27 to -0.73 Gt/yr), and North Pacific (-0.17 to -0.48 Gt/yr) are the largest sinks of CO_2 throughout the year (see Tables 1, 2, and 3). The North Pacific becomes a weak source (0.02 to 0.13 Gt/yr) of CO_2 during the Boreal summer (July-August). The equatorial Pacific is the largest source of CO_2 (0.28 to 0.81 Gt/yr) with positive values throughout the year. The largest flux in the equatorial Pacific is obtained with the Tans *et al.* (1990) algorithm and SSM/I winds. The Indian Ocean and the equatorial Atlantic are weak sources of CO_2 throughout the year (0.04 to 0.16 Gt/yr).

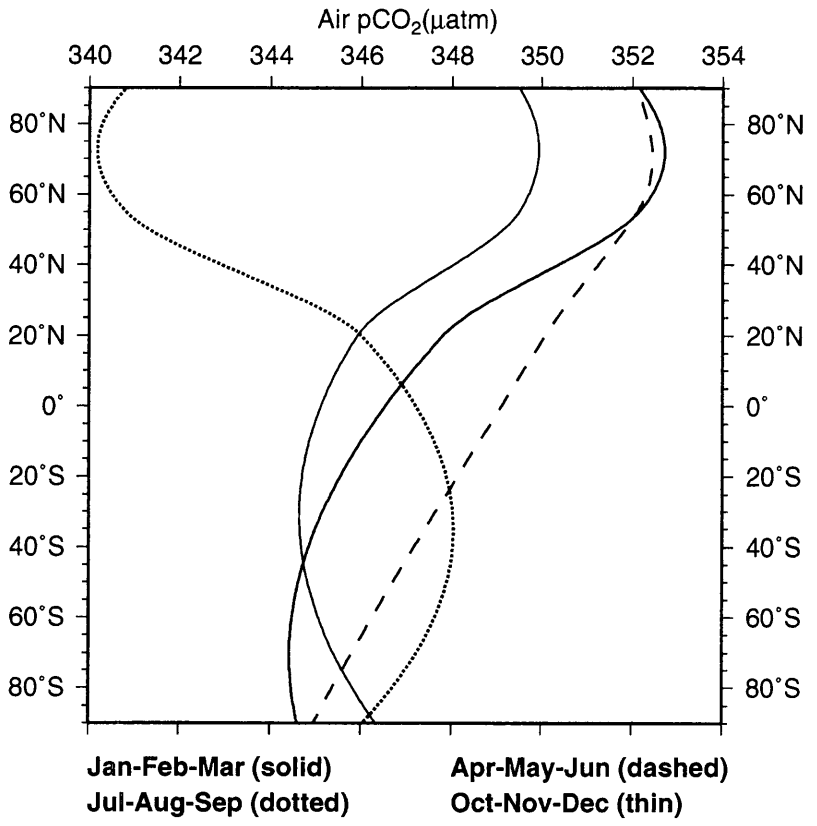

Figure 1. Latitude-dependent global seasonal distribution of atmospheric pCO_2 at one-degree resolution constructed by spline-fitting (Akima, 1970) three concurrently available records for 1990 (Conway and Tans, 1996): Cold Bay (55°N), Mauna Loa (19.5°N), and South Pole (90°S).

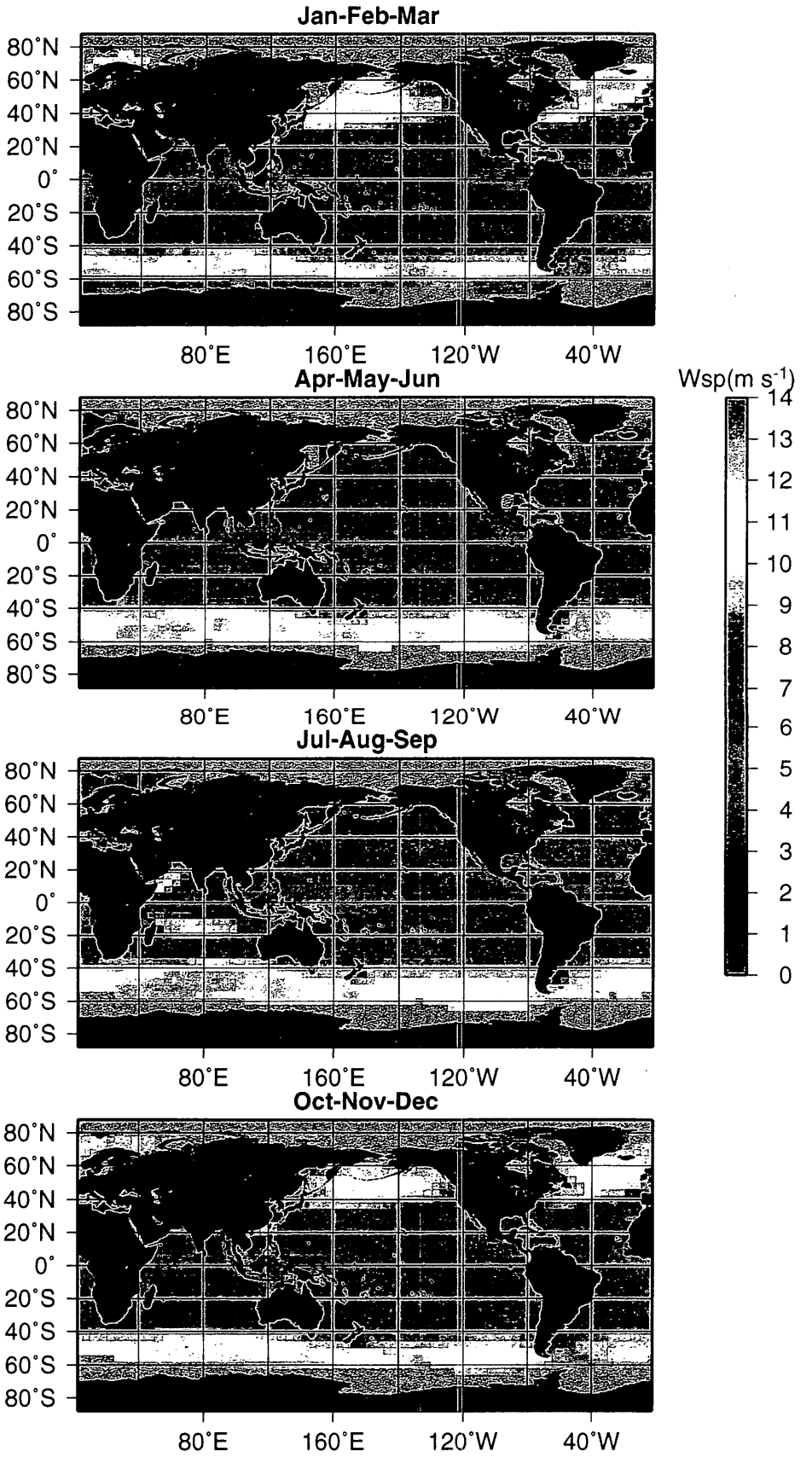

Figure 2. Seasonal wind speed fields from European Remote Sensing (ERS) Satellites climatology.

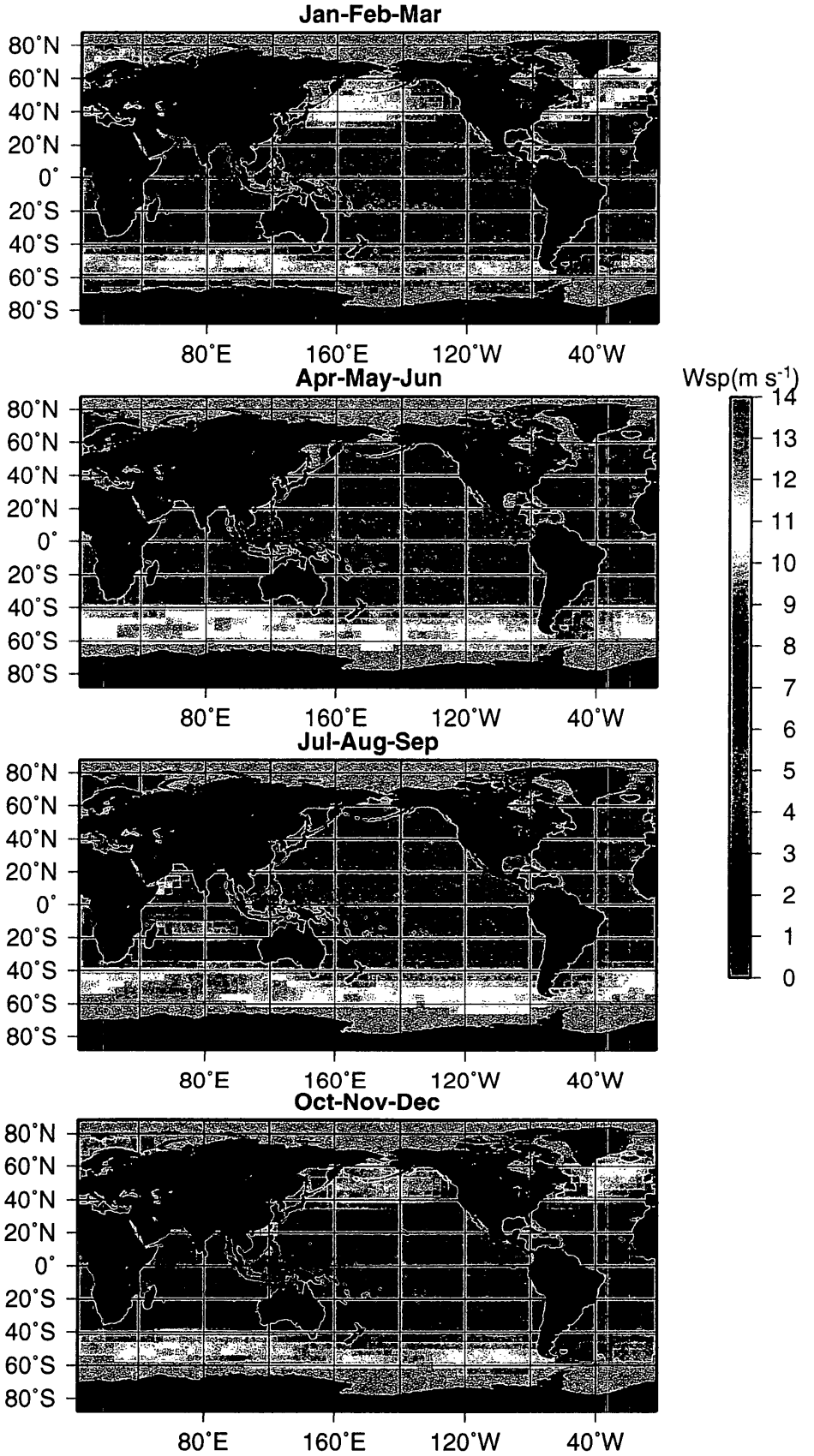

Figure 3. Seasonal wind speed fields from European Remote Sensing (ERS) Satellites climatology.

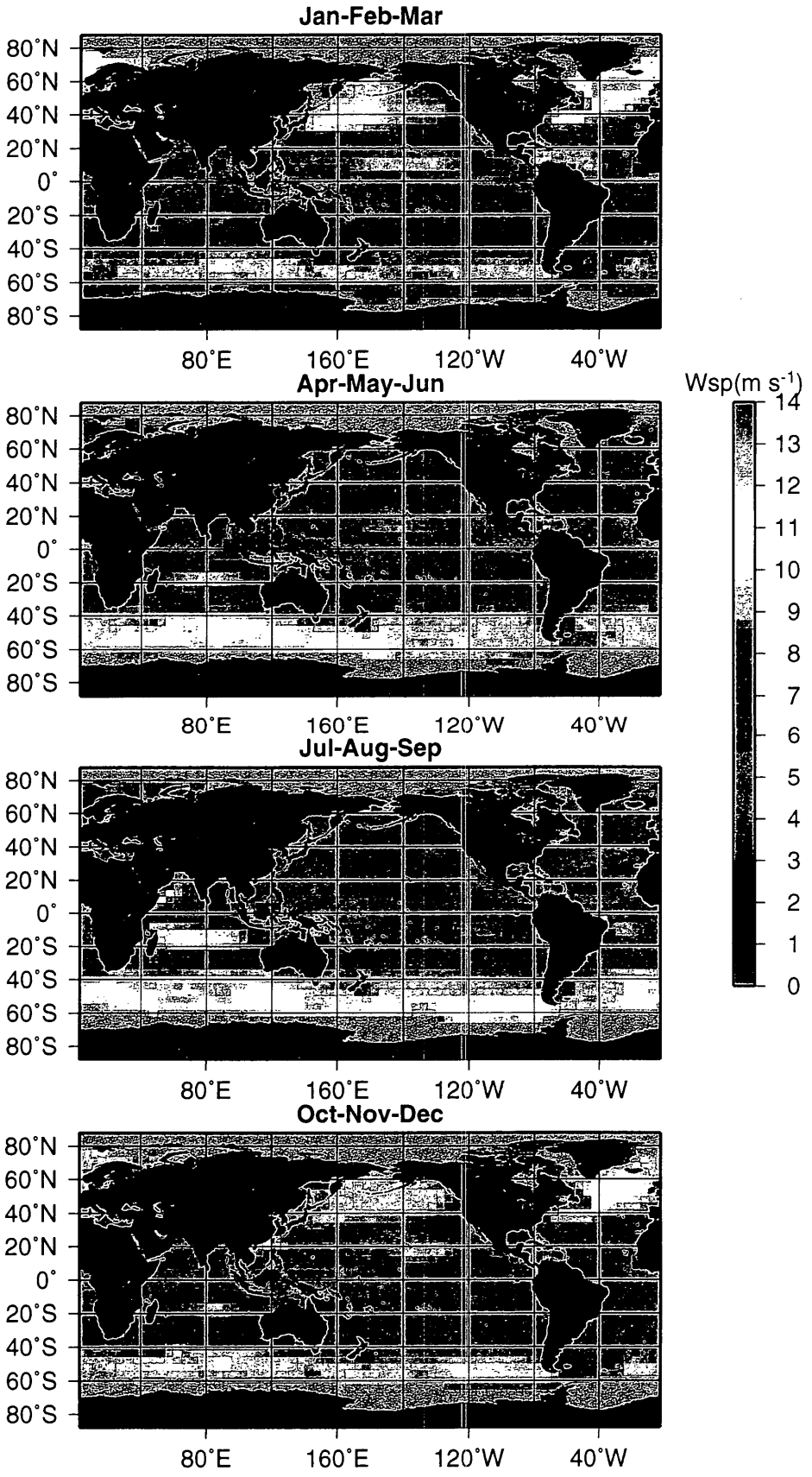

Figure 4. Seasonal wind speed fields from the Special Sensor Microwave/Imager (SSM/I) climatology. The SSM/I wind speed algorithm is described in Wentz (1997).

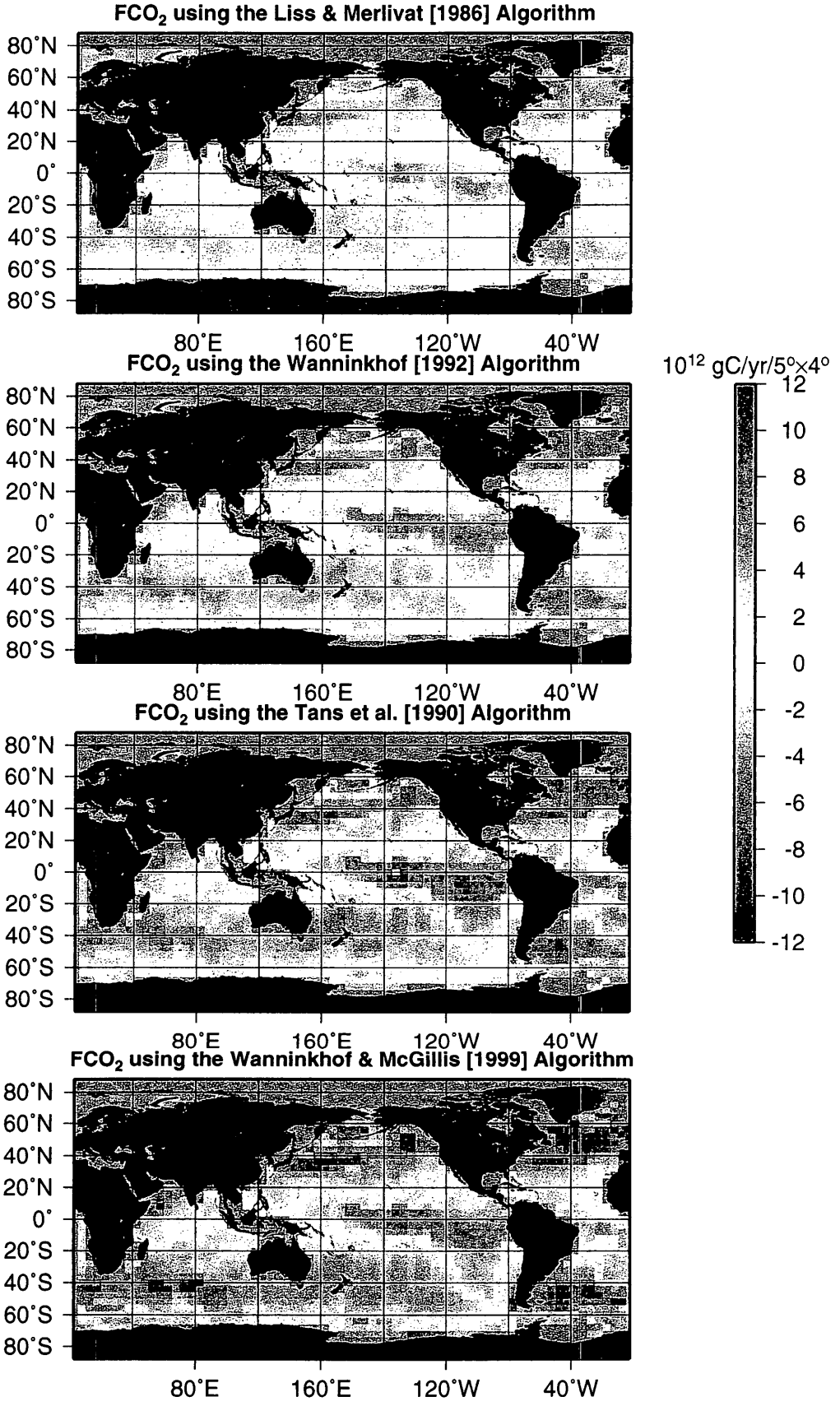

Figure 5. Global sea-air CO_2 flux derived with four different gas transfer algorithms and Esbensen and Kushnir (1981) winds.

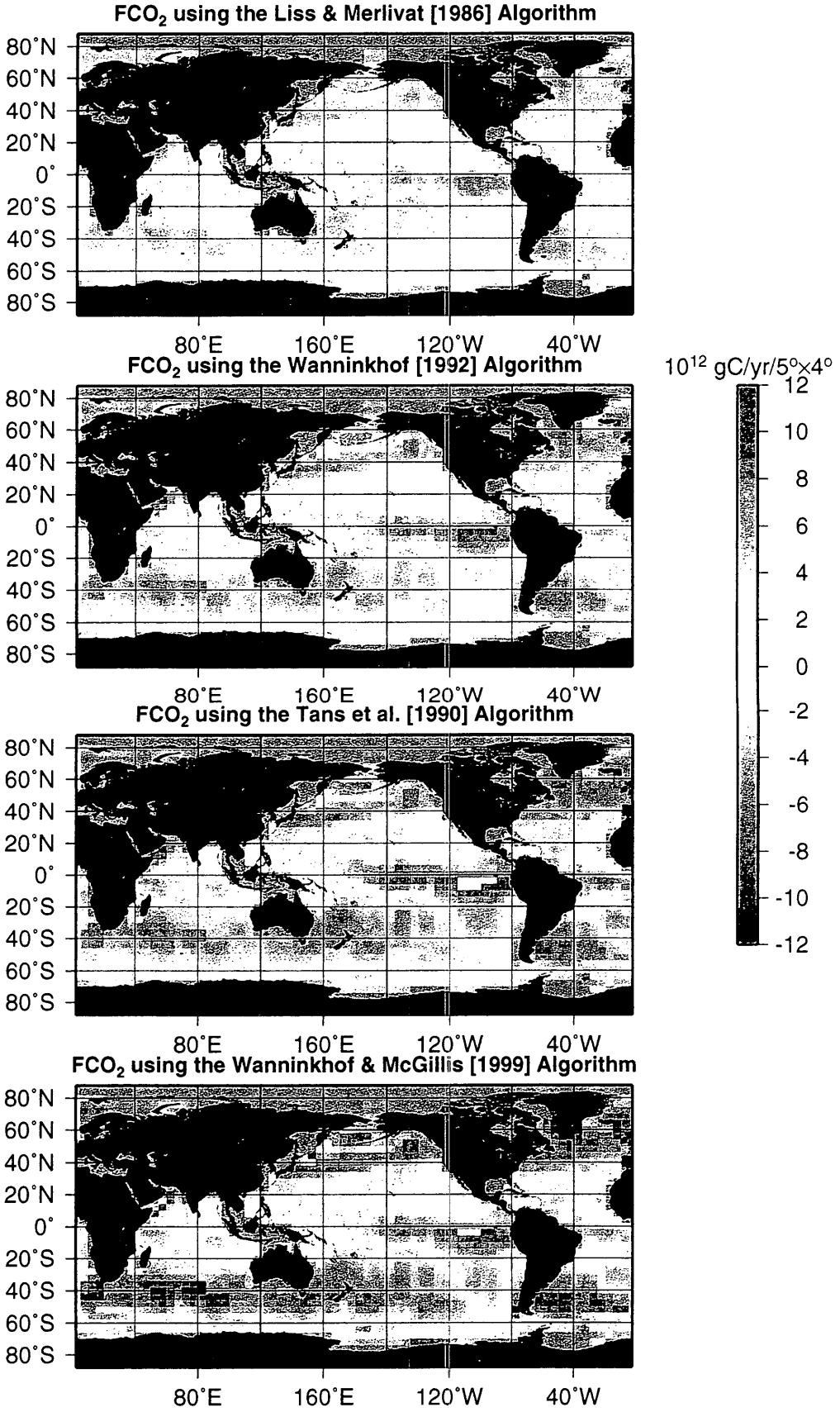

Figure 6. Global sea-air CO_2 flux derived with four different gas transfer algorithms and ERS scatterometer winds.

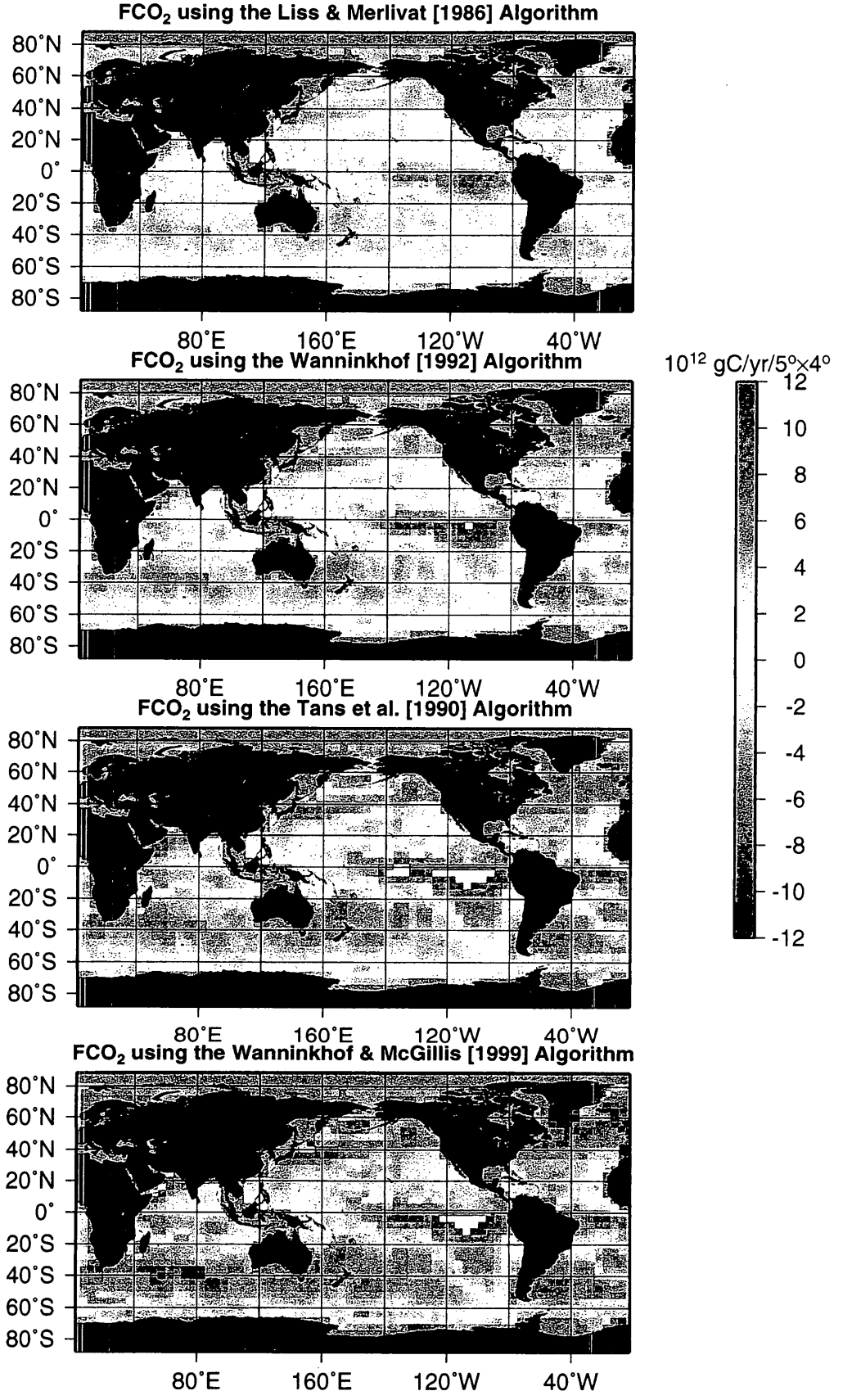

Figure 7. Global sea-air CO_2 flux derived with four different gas transfer algorithms and SSM/I winds.

Table 1. Sea-air CO_2 flux (Gt/yr) for the global oceans and for 6 regional oceanic domains. The estimates are from four different gas transfer algorithms and using climatological wind speeds from Esbensen and Kushnir (1981).

LM86	Jan	Feb	Mar	Apr	May	Jun	Jul	Aug	Sep	Oct	Nov	Dec	Year
Global Oceans	-0.85	-1.25	-1.22	-0.62	-0.36	-0.31	-0.14	-0.23	-0.45	-0.72	-0.82	-0.88	-0.65
Southern Ocean	-0.71	-1.10	-0.98	-0.47	-0.32	-0.50	-0.50	-0.44	-0.43	-0.46	-0.50	-0.60	-0.58
North Atlantic	-0.36	-0.35	-0.35	-0.32	-0.27	-.018	-0.11	-0.11	-0.17	-0.28	-0.37	-0.40	-0.27
Indian Ocean	0.06	0.04	0.02	0.00	0.01	0.07	0.08	0.07	0.05	0.00	0.01	0.03	0.04
Equatorial Atlantic	0.04	0.06	0.04	0.03	0.04	0.04	0.04	0.04	0.02	0.03	0.04	0.04	0.04
North Pacific	-0.33	-0.33	-0.32	-0.28	-0.21	-0.12	0.02	0.05	-0.02	-0.16	-0.27	-0.34	-0.19
Equatorial Pacific	0.36	0.30	0.24	0.27	0.29	0.31	0.31	0.26	0.24	0.22	0.24	0.30	0.28

W92	Jan	Feb	Mar	Apr	May	Jun	Jul	Aug	Sep	Oct	Nov	Dec	Year
Global Oceans	-1.37	-1.96	-1.89	-0.90	-0.50	-0.50	-0.23	-0.36	-0.68	-1.11	-1.32	-1.43	-1.02
Southern Ocean	-1.10	-1.72	-1.58	-0.75	-0.50	-0.82	-0.81	-0.70	-0.68	-0.72	-0.79	-0.93	-0.92
North Atlantic	-0.61	-0.59	-0.55	-0.49	-0.40	-0.27	-0.17	-0.17	-0.26	-0.44	-0.60	-0.66	-0.43
Indian Ocean	0.10	0.07	0.06	0.04	0.03	0.11	0.13	0.11	0.08	0.02	0.04	0.07	0.07
Equatorial Atlantic	0.06	0.10	0.07	0.06	0.06	0.06	0.06	0.06	0.04	0.05	0.06	0.06	0.06
North Pacific	-0.53	-0.51	-0.48	-0.42	-0.32	-0.18	0.03	0.08	-0.03	-0.25	-0.44	-0.56	-0.30
Equatorial Pacific	0.55	0.47	0.39	0.45	0.48	0.47	0.48	0.41	0.38	0.35	0.38	0.46	0.44

TANS90	Jan	Feb	Mar	Apr	May	Jun	Jul	Aug	Sep	Oct	Nov	Dec	Year
Global Oceans	-1.59	-2.37	-2.32	-1.17	-0.67	-0.56	-0.19	-0.38	-0.82	-1.37	-1.57	-1.67	-1.22
Southern Ocean	-1.45	-2.21	-1.95	-0.96	-0.69	-1.06	-1.05	-0.94	-0.92	-0.96	-1.05	-1.23	-1.21
North Atlantic	-0.78	-0.74	-0.73	-0.68	-0.59	-0.39	-0.24	-0.23	-0.35	-0.57	-0.75	-0.82	-0.57
Indian Ocean	0.14	0.10	0.06	0.02	0.04	0.15	0.17	0.16	0.11	0.02	0.04	0.09	0.09
Equatorial Atlantic	0.09	0.14	0.10	0.08	0.09	0.10	0.09	0.09	0.06	0.08	0.09	0.10	0.09
North Pacific	-0.70	-0.71	-0.68	-0.61	-0.47	-0.26	0.05	0.13	-0.03	-0.31	-0.55	-0.70	-0.40
Equatorial Pacific	0.83	0.70	0.56	0.66	0.71	0.72	0.72	0.61	0.58	0.53	0.57	0.69	0.66

WM99	Jan	Feb	Mar	Apr	May	Jun	Jul	Aug	Sep	Oct	Nov	Dec	Year
Global Oceans	-2.87	-3.67	-3.53	-1.76	-0.95	-1.08	-0.67	-0.75	-1.25	-2.09	-2.63	-2.95	-2.01
Southern Ocean	-1.65	-2.62	-2.64	-1.27	-0.76	-1.45	-1.37	-1.15	-1.05	-1.13	-1.22	-1.44	-1.48
North Atlantic	-1.17	-1.08	-0.91	-0.68	-0.50	-0.31	-0.18	-0.18	-0.36	-0.72	-1.04	-1.21	-0.70
Indian Ocean	0.09	0.06	0.05	0.02	0.00	0.19	0.25	0.17	0.07	0.01	0.02	0.06	0.08
Equatorial Atlantic	0.06	0.10	0.06	0.06	0.06	0.07	0.06	0.07	0.04	0.05	0.07	0.07	0.06
North Pacific	-0.90	-0.79	-0.68	-0.56	-0.38	-0.19	0.03	0.08	-0.07	-0.46	-0.81	-1.03	-0.48
Equatorial Pacific	0.61	0.50	0.41	0.47	0.47	0.47	0.49	0.41	0.38	0.34	0.38	0.48	0.45

The four gas transfer algorithms used are: LM86=Liss and Merlivat (1986); W92=Wanninkhof (1992); TANS90=Tans *et al.* (1990); and WM99=Wanninkhof and McGillis (1999).

The six oceanic regions are defined as follows:
Southern Ocean: south of 30°S
North Atlantic: 10°N to 80°N, and 100°W to 0°E
Indian Ocean: 30°S to 20°N, and 40°E to 100°E
Equatorial Atlantic: 10°S to 10°N, and 40°W to 0°E
North Pacific: 15°N to 65°N, and 120°E to 110°W
Equatorial Pacific: 10°S to 10°N, and 160°E to 75°W

Table 2. Sea-air CO_2 flux (Gt/yr) for the global oceans and for 6 regional oceanic domains. The estimates are from four different gas transfer algorithms and using SSM/I climatological wind speeds.

LM86	Jan	Feb	Mar	Apr	May	Jun	Jul	Aug	Sep	Oct	Nov	Dec	Year
Global Oceans	-0.71	-1.07	-1.03	-0.59	-0.33	-0.31	-0.08	-0.23	-0.41	-0.55	-0.71	-0.79	-0.57
Southern Ocean	-0.67	-1.10	-0.87	-0.47	-0.37	-0.56	-0.60	-0.52	-0.50	-0.51	-0.53	-0.59	-0.61
North Atlantic	-0.41	-0.39	-0.39	-0.36	-0.30	-0.22	-0.14	-0.12	-0.17	-0.25	-0.36	-0.44	-0.30
Indian Ocean	0.09	0.07	0.05	0.02	0.02	0.08	0.11	0.12	0.10	0.05	0.05	0.07	0.07
Equatorial Atlantic	0.06	0.09	0.07	0.06	0.06	0.06	0.07	0.06	0.04	0.05	0.06	0.06	0.06
North Pacific	-0.29	-0.28	-0.29	-0.28	-0.20	-0.13	0.03	0.06	-0.02	-0.12	-0.23	-0.31	-0.17
Equatorial Pacific	0.38	0.34	0.26	0.29	0.35	0.41	0.46	0.40	0.36	0.34	0.31	0.34	0.35

W92	Jan	Feb	Mar	Apr	May	Jun	Jul	Aug	Sep	Oct	Nov	Dec	Year
Global Oceans	-1.16	-1.69	-1.59	-0.85	-0.47	-0.52	-0.19	-0.38	-0.63	-0.86	-1.12	-1.29	-0.90
Southern Ocean	-1.02	-1.70	-1.37	-0.75	-0.58	-0.92	-0.99	-0.84	-0.80	-0.80	-0.82	-0.90	-0.96
North Atlantic	-0.68	-0.63	-0.62	-0.54	-0.45	-0.33	-0.21	-0.18	-0.25	-0.39	-0.58	-0.73	-0.47
Indian Ocean	0.14	0.12	0.10	0.06	0.04	0.13	0.19	0.19	0.15	0.09	0.09	0.11	0.12
Equatorial Atlantic	0.09	0.14	0.11	0.09	0.09	0.10	0.10	0.10	0.60	0.08	0.10	0.09	0.10
North Pacific	-0.45	-0.43	-0.43	-0.43	-0.30	-0.20	0.05	0.09	-0.03	-0.19	-0.36	-0.50	-0.26
Equatorial Pacific	0.58	0.53	0.41	0.47	0.56	0.62	0.70	0.61	0.55	0.52	0.48	0.52	0.55

TANS90	Jan	Feb	Mar	Apr	May	Jun	Jul	Aug	Sep	Oct	Nov	Dec	Year
Global Oceans	-1.32	-2.01	-1.94	-1.10	-0.61	-0.58	-0.08	-0.38	-0.73	-1.02	-1.34	-1.50	-1.05
Southern Ocean	-1.39	-2.22	-1.74	-0.98	-0.79	-1.17	-1.24	-1.09	-1.06	-1.06	-1.11	-1.23	-1.26
North Atlantic	-0.84	-0.80	-0.82	-0.76	-0.66	-0.48	-0.31	-0.25	-0.34	-0.52	-0.74	-0.91	-0.62
Indian Ocean	0.20	0.17	0.12	0.06	0.05	0.17	0.23	0.25	0.22	0.13	0.13	0.16	0.16
Equatorial Atlantic	0.14	0.22	0.16	0.14	0.13	0.14	0.14	0.14	0.08	0.12	0.14	0.14	0.14
North Pacific	-0.62	-0.62	-0.63	-0.61	-0.44	-0.28	0.08	0.13	-0.03	-0.25	-0.47	-0.64	-0.37
Equatorial Pacific	0.87	0.78	0.60	0.68	0.83	0.93	1.03	0.89	0.82	0.77	0.70	0.78	0.81

WM99	Jan	Feb	Mar	Apr	May	Jun	Jul	Aug	Sep	Oct	Nov	Dec	Year
Global Oceans	-2.39	-3.06	-2.90	-1.61	-0.93	-1.10	-0.62	-0.71	-1.10	-1.59	-2.12	-2.59	-1.73
Southern Ocean	-1.43	-2.49	-2.17	-1.24	-0.95	-1.66	-1.82	-1.46	-1.30	-1.27	-1.25	-1.31	-1.53
North Atlantic	-1.26	-1.10	-0.99	-0.74	-0.55	-0.39	-0.24	-0.21	-0.34	-0.59	-0.97	-1.33	-0.73
Indian Ocean	0.15	0.12	0.09	0.05	0.01	0.23	0.36	0.34	0.22	0.11	0.09	0.12	0.16
Equatorial Atlantic	0.11	0.16	0.12	0.11	0.11	0.13	0.14	0.13	0.08	0.11	0.13	0.12	0.12
North Pacific	-0.69	-0.59	-0.55	-0.56	-0.34	-0.22	0.07	0.10	-0.06	-0.30	-0.59	-0.84	-0.38
Equatorial Pacific	0.64	0.59	0.43	0.52	0.61	0.73	0.91	0.77	0.68	0.63	0.55	0.59	0.64

The four gas transfer algorithms used are: LM86=Liss and Merlivat (1986); W92=Wanninkhof (1992); TANS90=Tans *et al.* (1990); and WM99=Wanninkhof and McGillis (1999).

The six oceanic regions are defined as follows:
Southern Ocean: south of 30°S
North Atlantic: 10°N to 80°N, and 100°W to 0°E
Indian Ocean: 30°S to 20°N, and 40°E to 100°E
Equatorial Atlantic: 10°S to 10°N, and 40°W to 0°E
North Pacific: 15°N to 65°N, and 120°E to 110°W
Equatorial Pacific: 10°S to 10°N, and 160°E to 75°W

Table 3. Sea-air CO_2 flux (Gt/yr) for the global oceans and for 6 regional oceanic domains. The estimates are from four different gas transfer algorithms and using ERS climatological wind speeds.

LM86	Jan	Feb	Mar	Apr	May	Jun	Jul	Aug	Sep	Oct	Nov	Dec	Year
Global Oceans	-0.84	-1.22	-1.23	-0.68	-0.43	-0.40	-0.17	-0.32	-0.57	-0.73	-0.85	-0.91	-0.70
Southern Ocean	-0.76	-1.16	-1.02	-0.55	-0.42	-0.58	-0.63	-0.57	-0.57	-0.58	-0.61	-0.67	-0.67
North Atlantic	-0.39	-0.37	-0.38	-0.35	-0.31	-0.23	-0.15	-0.11	-0.18	-0.29	-0.37	-0.41	-0.30
Indian Ocean	0.08	0.07	0.05	0.03	0.03	0.09	0.11	0.11	0.08	0.04	0.04	0.06	0.07
Equatorial Atlantic	0.05	0.07	0.06	0.05	0.05	0.05	0.06	0.05	0.03	0.05	0.05	0.05	0.05
North Pacific	-0.26	-0.25	-0.27	-0.26	-0.20	-0.15	0.02	0.04	-0.04	-0.15	-0.24	-0.30	-0.17
Equatorial Pacific	0.33	0.29	0.23	0.26	0.32	0.37	0.42	0.35	0.31	0.29	0.27	0.31	0.31

W92	Jan	Feb	Mar	Apr	May	Jun	Jul	Aug	Sep	Oct	Nov	Dec	Year
Global Oceans	-1.36	-1.92	-1.93	-1.03	-0.66	-0.66	-0.34	-0.55	-0.91	-1.19	-1.39	-1.50	-1.12
Southern Ocean	-1.18	-1.82	-1.64	-0.91	-0.70	-0.96	-1.06	-0.95	-0.93	-0.95	-0.98	-1.06	-1.10
North Atlantic	-0.65	-0.60	-0.60	-0.54	-0.46	-0.34	-0.22	-0.17	-0.28	-0.46	-0.59	-0.68	-0.47
Indian Ocean	0.13	0.11	0.09	0.06	0.05	0.15	0.20	0.18	0.13	0.08	0.08	0.10	0.11
Equatorial Atlantic	0.08	0.11	0.09	0.08	0.08	0.08	0.08	0.08	0.51	0.07	0.08	0.08	0.08
North Pacific	-0.40	-0.38	-0.40	-0.39	-0.30	-0.22	0.03	0.07	-0.06	-0.23	-0.39	-0.49	-0.26
Equatorial Pacific	0.51	0.45	0.37	0.44	0.51	0.56	0.63	0.52	0.48	0.44	0.41	0.47	0.48

TANS90	Jan	Feb	Mar	Apr	May	Jun	Jul	Aug	Sep	Oct	Nov	Dec	Year
Global Oceans	-1.58	-2.30	-2.34	-1.28	-0.80	-0.73	-0.25	-0.56	-1.03	-1.37	-1.62	-1.73	-1.30
Southern Ocean	-1.55	-2.33	-2.02	-1.12	-0.89	-1.21	-1.30	-1.18	-1.17	-1.19	-1.25	-1.38	-1.38
North Atlantic	-0.80	-0.76	-0.79	-0.75	-0.66	-0.49	-0.32	-0.24	-0.37	-0.59	-0.75	-0.85	-0.61
Indian Ocean	0.19	0.16	0.12	0.07	0.07	0.19	0.25	0.24	0.19	0.11	0.11	0.14	0.15
Equatorial Atlantic	0.12	0.17	0.13	0.12	0.12	0.12	0.12	0.12	0.08	0.10	0.12	0.12	0.12
North Pacific	-0.56	-0.56	-0.60	-0.57	-0.44	-0.32	0.04	0.11	-0.07	-0.30	-0.49	-0.63	-0.37
Equatorial Pacific	0.77	0.67	0.54	0.63	0.76	0.85	0.94	0.79	0.72	0.66	0.62	0.72	0.72

WM99	Jan	Feb	Mar	Apr	May	Jun	Jul	Aug	Sep	Oct	Nov	Dec	Year
Global Oceans	-2.76	-3.56	-3.63	-2.11	-1.39	-1.40	-1.02	-1.21	-1.83	-2.41	-2.80	-3.08	-2.27
Southern Ocean	-1.83	-2.86	-2.80	-1.67	-1.28	-1.79	-2.05	-1.78	-1.70	-1.69	-1.65	-1.71	-1.90
North Atlantic	-1.19	-1.04	-0.97	-0.75	-0.57	-0.40	-0.25	-0.20	-0.41	-0.74	-1.02	-1.24	-0.73
Indian Ocean	0.13	0.11	0.09	0.05	0.03	0.27	0.40	0.31	0.17	0.08	0.07	0.10	0.15
Equatorial Atlantic	0.08	0.11	0.09	0.09	0.09	0.10	0.11	0.10	0.07	0.09	0.10	0.09	0.09
North Pacific	-0.55	-0.47	-0.48	-0.48	-0.33	-0.26	0.03	0.07	-0.11	-0.40	-0.65	-0.84	-0.37
Equatorial Pacific	0.53	0.46	0.36	0.44	0.52	0.61	0.75	0.61	0.53	0.48	0.44	0.51	0.52

The four gas transfer algorithms used are: LM86=Liss and Merlivat (1986); W92=Wanninkhof (1992); TANS90=Tans *et al.* (1990); and WM99=Wanninkhof and McGillis (1999).

The six oceanic regions are defined as follows:
Southern Ocean: south of 30°S
North Atlantic: 10°N to 80°N, and 100°W to 0°E
Indian Ocean: 30°S to 20°N, and 40°E to 100°E
Equatorial Atlantic: 10°S to 10°N, and 40°W to 0°E
North Pacific: 15°N to 65°N, and 120°E to 110°W
Equatorial Pacific: 10°S to 10°N, and 160°E to 75°W

Monthly time series for the global oceans and six regional domains are shown for all wind speed data sets and gas transfer algorithms in Figures 8, 9, and 10. The Southern Ocean has the largest seasonal cycle with a peak in ocean uptake during January - February. The North Atlantic and North Pacific Oceans have a reduced seasonal cycle, with strongest uptake during fall-winter and nearly neutral conditions during the summer months. These regions have small outgassing (North Pacific) or small ingassing (North Atlantic) of CO_2 during the summer months because the potentially high pCO_2 values due to elevated SST conditions are counterbalanced by an increased pCO_2 drawdown by biological activity. The Indian Ocean, equatorial Pacific, and equatorial Atlantic have no distinctive seasonal cycle.

Table 4. Average wind speeds for the global oceans and 6 regional oceanic domains. The tabulated values are presented for three different wind climatologies: Esbensen and Kushnir (1981), ERS, and SSM/I.

Wind Climatology	Esbensen and Kushnir (1981)	ERS	SSM/I
Global Oceans	7.1	7.3	7.2
Southern Ocean	9.1	9.6	9.0
North Atlantic	7.4	7.3	7.4
Indian Ocean	5.9	6.3	6.6
Equatorial Atlantic	5.7	6.2	6.7
North Pacific	7.5	7.4	7.3
Equatorial Pacific	5.7	5.8	6.2

The six oceanic regions are defined as follows:
Southern Ocean: south of 30°S
North Atlantic: 10°N to 80°N, and 100°W to 0°E
Indian Ocean: 30°S to 20°N, and 40°E to 100°E
Equatorial Atlantic: 10°S to 10°N, and 40°W to 0°E
North Pacific: 15°N to 65°N, and 120°E to 110°W
Equatorial Pacific: 10°S to 10°N, and 160°E to 75°W

Our CO_2 flux estimates agree well with the estimates of Takahashi *et al.* (1997) using Esbensen and Kushnir (1981) winds. Their estimates using the Liss and Merlivat (1986), Wanninkhof (1992), and Wanninkhof and McGillis (1999) gas transfer algorithms are -0.60, -1.01, and -1.17 Gt/yr, respectively. Our equivalent estimates are -0.65, -1.02, and -1.22 Gt/yr.

Lefèvre *et al.* (1999) assessed the seasonality of the oceanic sink for CO_2 in the northern hemisphere. They compiled quarterly maps of ΔpCO_2 interpolated from pCO_2 measurements in the North Atlantic and the North Pacific Oceans using an objective mapping technique. Their estimates of the CO_2 flux for the Northern Hemisphere north of 10°N using SSM/I winds and the Liss and Merlivat (1986), Wanninkhof (1992), and Tans *et al.* (1990) algorithms are -0.45, -0.70, and -0.86 Gt/yr, respectively. Our equivalent estimates are -0.52, -0.81, and -1.08 Gt/yr. Lefèvre *et al.* (1999) estimates using Esbensen and Kushnir (1981) winds using the same three gas transfer algorithms are -0.37, -0.60, and -0.76 Gt/yr, respectively. Our equivalent estimates are -0.50, -0.78, -1.03 Gt/yr. Overall, our estimates are 15% to 35% higher than those of Lefèvre *et al.* (1999). Since we used pCO_2 data based on Takahashi *et al.* (1997), and Lefèvre *et al.* (1999) used revised pCO_2 maps based on additional observations, we attributed our CO_2 flux overestimates to the different pCO_2 data sets used for the estimates.

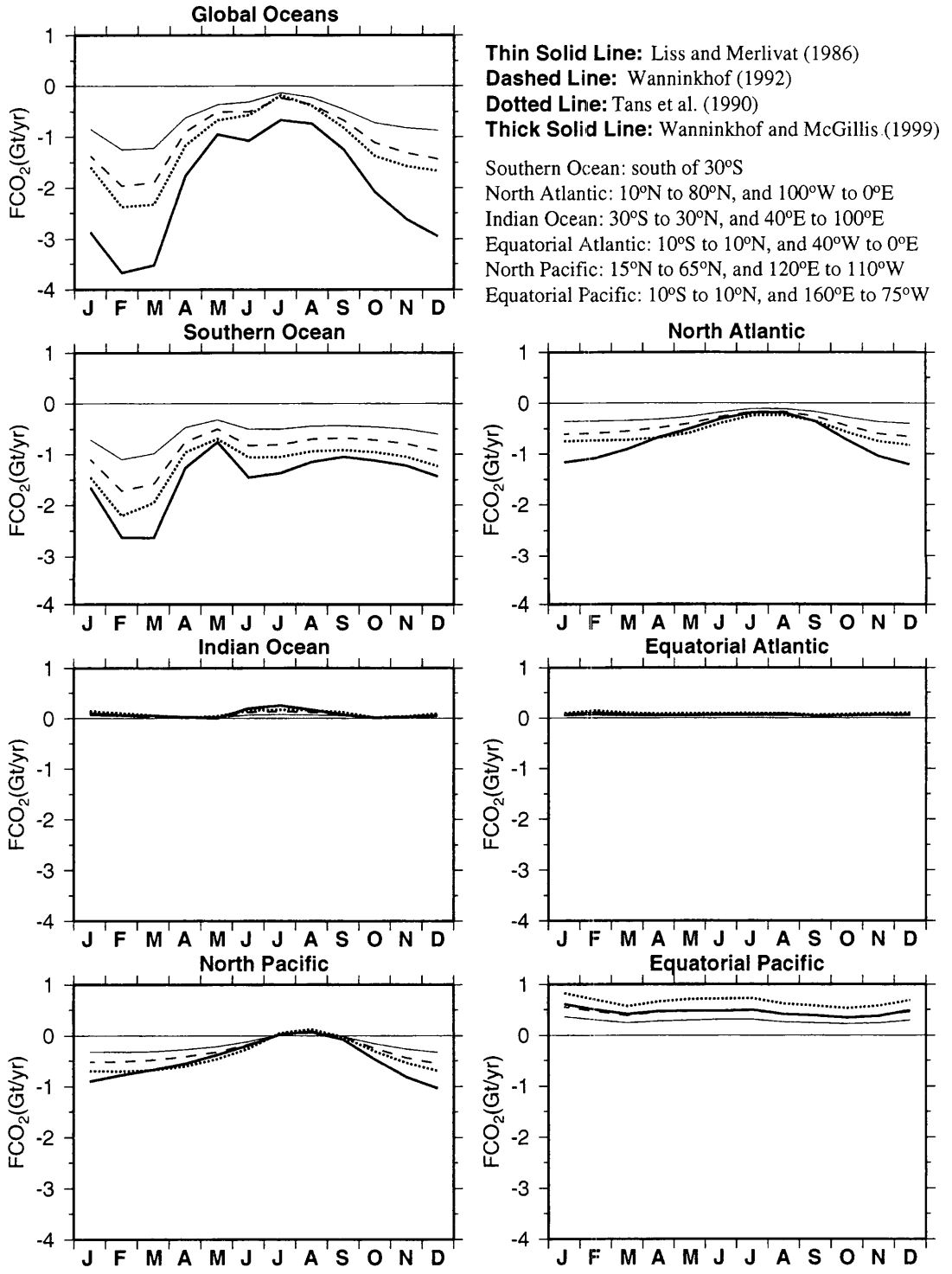

Figure 8. Seasonal variability of sea-air CO_2 flux derived with Esbensen and Kushnir (1981) winds for the global oceans and six different oceanic regions. The four separate lines (solid, dashed, dotted, and thick solid) represent the respective gas transfer algorithms used.

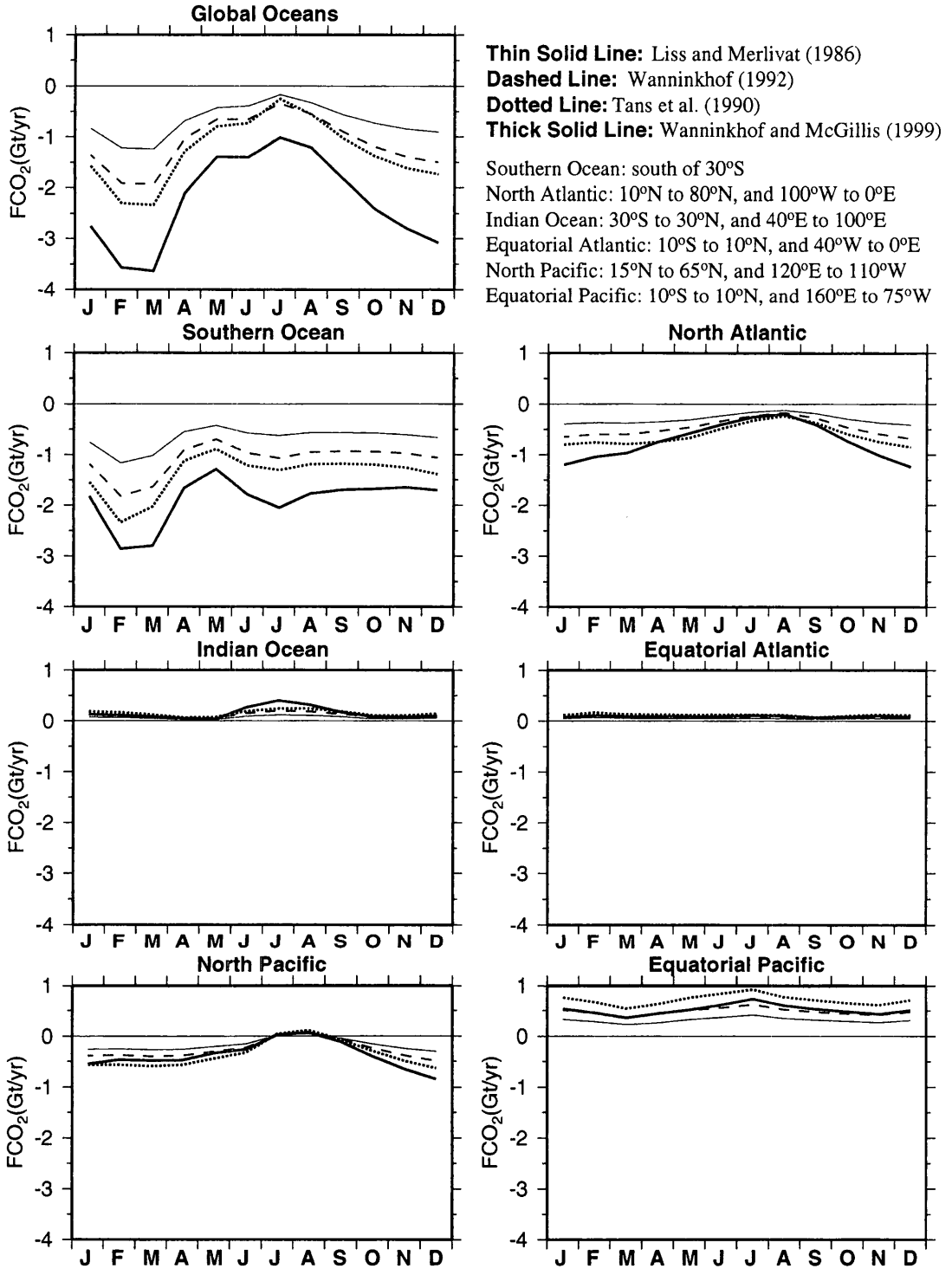

Figure 9. Seasonal variability of sea-air CO_2 flux derived with ERS winds for the global oceans and six different oceanic regions. The four separate lines (solid, dashed, dotted, and thick solid) represent the respective gas transfer algorithms used.

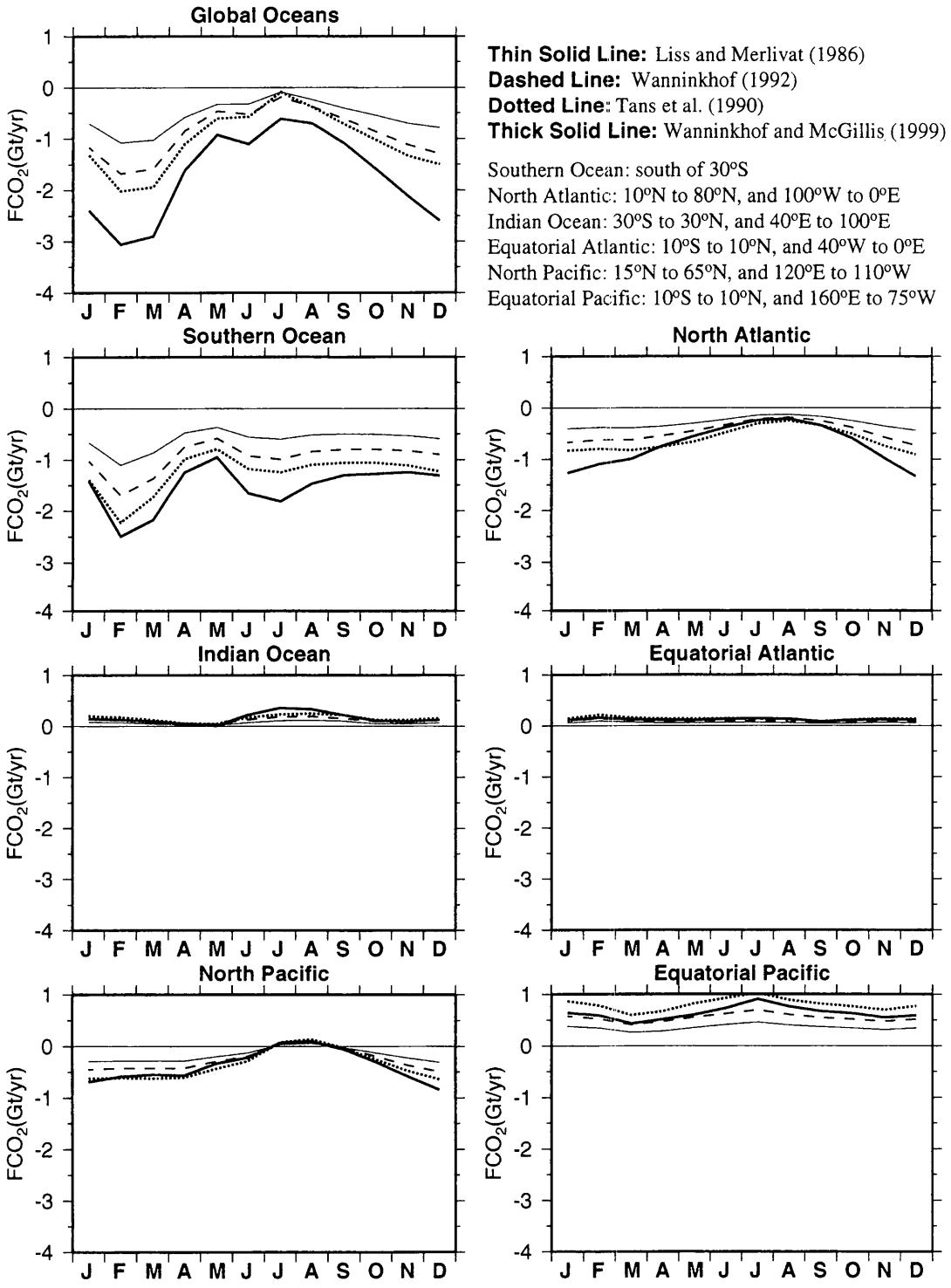

Figure 10. Seasonal variability of sea-air CO_2 flux derived with SSM/I winds for the global oceans and six different oceanic regions. The four separate lines (solid, dashed, dotted, and thick solid) represent the respective gas transfer algorithms used.

4. Sensitivity to SST and SSS

As mentioned in Section 2, sensitivity analyses were conducted with different SST and SSS inputs. The Tans *et al.* (1990) gas transfer algorithm was used in all cases. Variability in SST and SSS global distributions affect the calculation of TA (Millero *et al.*, 1998), CO_2 solubility, the Schmidt number, and the ocean pCO_2 via the dissociation constants for carbonic acid, boric acid, and sea water, which all combined affect the sea-air CO_2 flux. The World Ocean Atlas 1998 SST and SSS data are used as a reference calculation to be compared with the results of other sea-air flux calculations using different combinations of SST and SSS. The results are summarized in Table 5. Figure 11 shows the global distribution of the sea-air CO_2 flux using two different combinations of SST and SSS monthly fields, World Ocean Atlas 1998 SST and SSS (top plate), and Reynolds and Smith (1994) SST and World Ocean Atlas 1998 SSS (middle plate). The bottom plate shows the differences between the two SST and SSS combinations. The differences are relatively large, ranging from -4 to +4 Gt/yr. Globally, the mean ocean uptake of CO_2 is 35% larger when the Reynolds and Smith (1994) SST data are used, and the seasonal range is 17% larger.

Table 5. Sensitivity of sea-air global CO_2 flux (in Gt/yr) to SST and SSS climatologies. Tabulated values show the mean and seasonal range for various combinations of SST and SSS climatologies. Tabulated values for salinity biases of ±0.2 are also included. The differences in percent relative to the reference calculation (using SST and SSS from World Oceans Atlas 1998) are also shown. All estimates were obtained using the Tans *et al.* (1990) gas transfer algorithm and ERS wind speeds.

SST and SSS Sources	Mean	Difference(%)	Range	Difference(%)
WOA94 SST and SSS	-1.40	+0.8	13.5	+18.1
WOA94 SST and WOA98 SSS	-1.25	-4.2	13.4	+16.9
WOA98 SST and WOA94 SSS	-1.37	+5.1	11.6	+1.2
R&S94 SST and WOA98 SSS	-1.75	+34.7	13.4	+17.4
WOA98 SST and WOA98 SSS+0.2	-0.91	-42.8	11.3	-1.1
WOA98 SST and WOA98 SSS-0.2	-1.86	+42.7	11.6	+1.3

The annual mean and seasonal range for the reference calculation are -1.30 Gt/yr and 11.4 Gt/yr, respectively. The mean SST and SSS deviations between the WOA98 and WOA94 climatologies are -0.05 ±0.61 °C and 0.18 ±1.41, respectively. The mean SST deviation between the WOA98 and R&S94 climatologies is 0.24 ±3.42 °C.

WOA98: World Ocean Atlas 1998 (Conkright *et al.*, 1998)
WOA94: World Ocean Atlas 1994 (Levitus and Boyer, 1994; Levitus *et al.*, 1994)
R&S94: High-resolution global sea surface temperature climatology (Reynolds and Smith, 1994)

The use of both SST and SSS from the World Ocean Atlas 1994 data causes an increase in ocean uptake of only 0.8%, but the seasonal range increases 18% (Figure 12 and Table 5). The combination of World Ocean Atlas 1998 SST and World Ocean Atlas 1994 SSS causes an increase of 5% in CO_2 uptake, with a slight increase of seasonal range (1%).

The last sensitivity test is conducted with the inclusion of a salinity bias on the SSS seasonal fields. The bias was chosen to be ±0.2, in the context of remote sensing instrument accuracy.

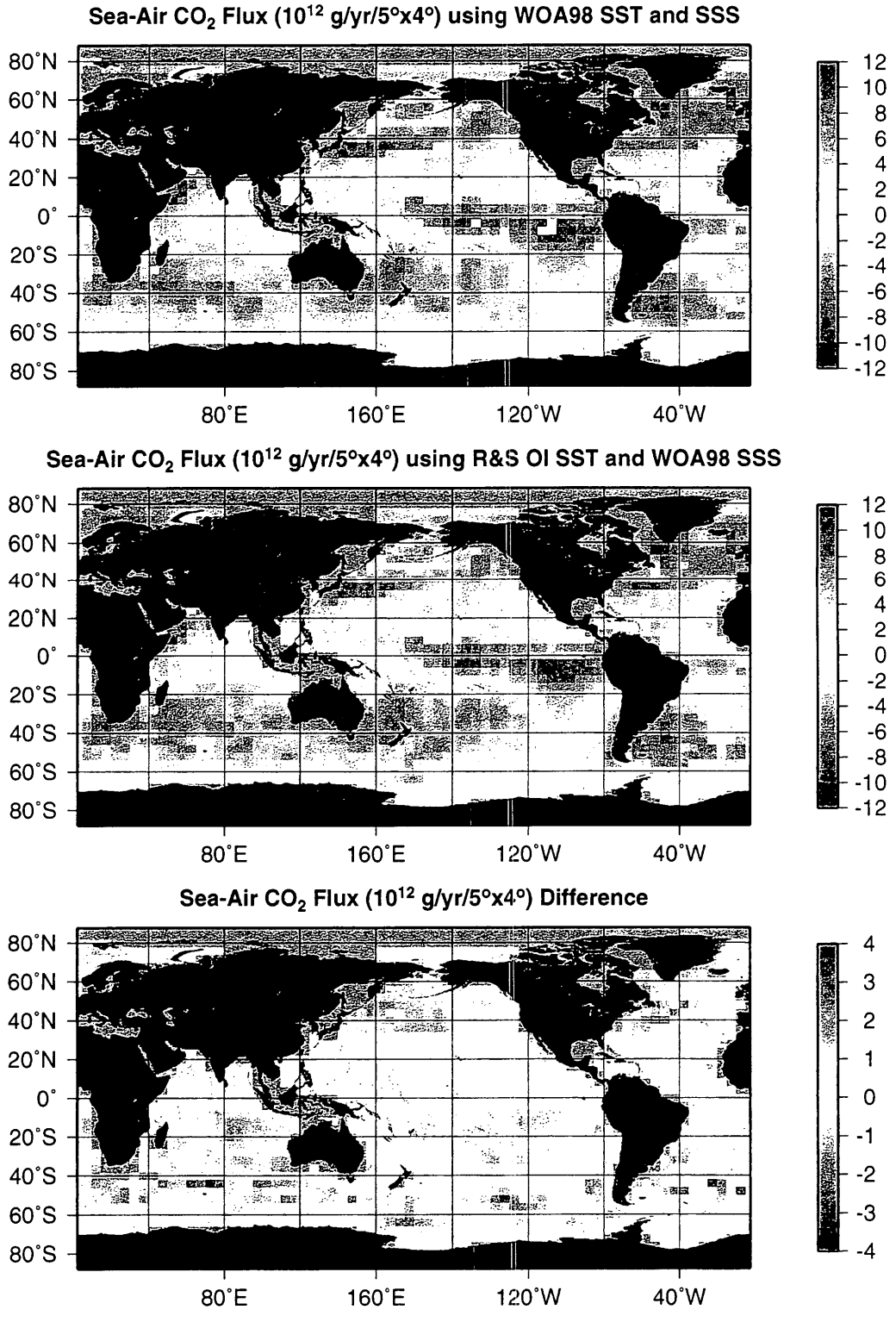

Figure 11. Global sea-air CO_2 flux derived with the Tans *et al.* (1990) gas transfer algorithm and two different combinations of SST and SSS fields: World Ocean Atlas 1998 SST and SSS (top panel), and Reynolds and Smith (1994) SST and World Ocean Atlas 1998 SSS (middle panel). The bottom panel shows the difference between the top panel and the middle panel flux distributions.

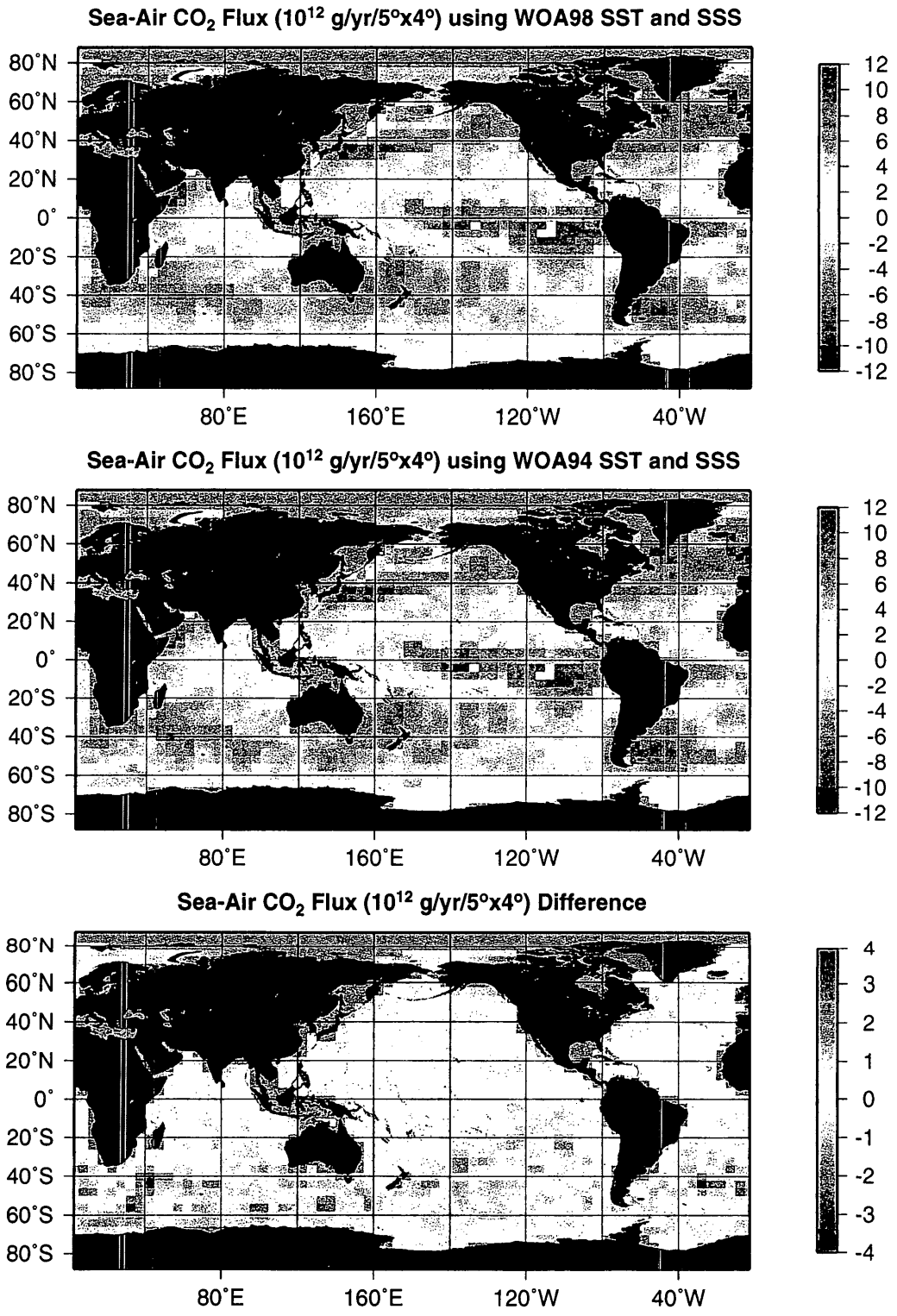

Figure 12. Global sea-air CO_2 flux derived with the Tans *et al.* (1990) gas transfer algorithm and two different combinations of SST and SSS fields: World Ocean Atlas 1998 SST and SSS (top panel), and World Ocean Atlas 1994 SST and SSS (middle panel). The bottom panel shows the difference between the top panel and the middle panel flux distributions.

This bias may be related to skin versus bulk salinity retrievals, and to some extent related to the mission specifications. Table 5 shows that the ±0.2 bias in salinity causes an error of ±43% on the mean global CO_2 flux, and a change of ±1% on the seasonal range. This result shows that relatively small changes in salinity cause large changes in the global sea-air flux, posing a significant challenge for future remote sensing salinity missions aimed at helping the development of global sea-air CO_2 flux algorithms. This study also indicates the potential impacts of changes in the oceanic hydrologic cycle on CO_2 fluxes, although salinity changes would be regional and could be either positive or negative. SSS changes in regions of high flux could be significant to the global CO_2 flux.

5. Summary and Conclusions

We used an ocean pCO_2 model (Signorini *et al.*, 2001a; Signorini *et al.*, 2001b), combined with algorithms for TA and gas transfer, to estimate the seasonal sea-air CO_2 flux for the global oceans. Sensitivity analyses of sea-air CO_2 flux to wind speed climatologies, gas transfer algorithms, SSS and SST were conducted for the global oceans and regional domains.

The Liss and Merlivat (1986) gas transfer algorithm produces the smallest sea-air flux with all three wind speed climatologies. Using this algorithm, the global sea-air flux ranges from -0.57 Gt/yr using SSM/I winds, to -0.70 Gt/yr using ERS winds. The largest sea-air flux was obtained with the Wanninkhof and McGillis (1999) gas transfer algorithm, which yields -1.73 Gt/yr with SSM/I winds and -2.27 Gt/yr with ERS winds. . The Southern Ocean (-0.58 to -1.48 Gt/yr), North Atlantic (-0.27 to -0.73 Gt/yr), and North Pacific (-0.17 to -0.48 Gt/yr) are the largest sinks of CO_2 throughout the year. The equatorial Pacific is the largest source of CO_2 (0.28 to 0.81 Gt/yr) with positive values throughout the year. The largest flux in the equatorial Pacific is obtained with the Tans *et al.* (1990) algorithm and SSM/I winds. The Indian Ocean and the equatorial Atlantic are weak sources of CO_2 throughout the year (0.04 to 0.16 Gt/yr).

The Southern Ocean has the largest seasonal cycle with a peak in ocean uptake during January-February (-1.10 to -2.86 Gt/yr). The North Atlantic and North Pacific Oceans have a reduced seasonal cycle, with strongest uptake during fall-winter and nearly neutral conditions during the summer months. These regions have small outgassing (North Pacific) or small ingassing (North Atlantic) of CO_2 during the summer months because the potentially high pCO_2 values due to elevated SST conditions are compensated by an increased pCO_2 drawdown by biological activity. The Indian Ocean, equatorial Pacific, and equatorial Atlantic have no distinctive seasonal cycle.

The sensitivity of sea-air flux to SST and SSS was conducted with several climatological combinations. Data from the World Ocean Atlas 1998 was assumed as a reference calculation for the other SST and SSS combinations. Globally, the mean ocean uptake of CO_2 is 35% larger when the Reynolds and Smith (1994) SST data are used in combination with SSS from the World Ocean Atlas 1998. The seasonal range with this SST and SSS combination is 17% larger. The use of both SST and SSS from the World Ocean Atlas 1994 data causes an increase in ocean uptake of only 0.8%, but the seasonal range increases 18%. The combination of World Ocean

Atlas 1998 SST and World Ocean Atlas 1994 SSS causes an increase of 5% in CO_2 uptake, with a slight increase of seasonal range (1%).

An additional sensitivity test was conducted with the inclusion of a salinity bias on the SSS seasonal fields. The bias was chosen to be ±0.2, which is assumed to be related to instrument error and/or limitations (for example, skin versus bulk salinity retrievals). The ±0.2 bias in salinity causes an error of ±43% on the mean global CO_2 flux, and a relatively small change of ±1% on the seasonal range. This result shows that small changes in salinity (< 1%) cause large changes in the global sea-air flux, posing a significant challenge for future remote sensing salinity missions aimed at helping the development global sea-air CO_2 flux algorithms.

References

Akima, H., 1970. A New Method of Interpolation and Smooth Curve Fitting Based on Local Procedures. J. ACM 17, 589-602.

Antoine, D., Morel, A., 1995. Modeling the Seasonal Course of the Upper Ocean Pco(2) .1. Development of a One-Dimensional Model. Tellus Ser. B-Chem. Phys. Meteorol. 47, 103-121.

Behrenfeld, M.J., Randerson, J.T., McClain, C.R., Feldman, G.C., Los, S.O., Tucker, C.J., Falkowski, P.G., Field, C.B., Frouin, R., Esaias, W.E., Kolber, D.D., Pollack, N.H., 2001. Biospheric primary production during an ENSO transition. Science 291, 2594-2597.

Broecker, W.S., Peng, T.-H., 1982. Tracers in the Sea. Eldigio, Palisades, New York.

Conkright, M., Levitus, S., O'Brien, T., Boyer, T., Antonov, J., Stephens, C., 1998. World Ocean Atlas 1998 CD-ROM Data Set Documentation. NODC Internal Report, Silver Spring, MD Tech. Rep. 15, 16 pp.

Conway, T.J., Tans, P.P., 1996. Atmospheric Carbon Dioxide Mixing Ratios from the NOAA Climate Monitoring and Diagnostics Laboratory Cooperative Flask Sampling Network, 1967-1993. ORNL/CDIAC-73, NDP-005/R3. Carbon Dioxide Information Analysis, Oak Ridge National Laboratory, Oak Ridge, Tennessee, pp. 202 pp.

Dickson, A.G., Millero, F.J., 1987. A Comparison of the Equilibrium-Constants for the Dissociation of Carbonic-Acid in Seawater Media. Deep-Sea Research Part a-Oceanographic Research Papers 34, 1733-1743.

Esbensen, S.K., Kushnir, V., 1981. The heat budget of the global ocean: An atlas based on estimates from surface marine observations. Tech. Rep. 29, Clim. Res. Inst. Oreg. State Univ., Corvallis.

Lagerloef, G., Swift, C., LeVine, D., 1995. Sea surface salinity: The next remote sensing challenge. Oceanography 8, 44-50.

Lee, K., Wanninkhof, R., Feely, R.A., Millero, F.J., Peng, T.H., 2000. Global relationships of total inorganic carbon with temperature and nitrate in surface seawater. Glob. Biogeochem. Cycle 14, 979-994.

Lefèvre, N., Watson, A.J., Cooper, D.J., Weiss, R.F., Takahashi, T., Sutherland, S.C., 1999. Assessing the seasonality of the oceanic sink for CO2 in the northern hemisphere. Glob. Biogeochem. Cycle 13, 273-286.

Levitus, S., Boyer, T., 1994. World Ocean Atlas 1994 Vol. 4: Temperature. NOAA Atlas NESDIS 4. U.S. Department of Commerce, Washington, D.C., pp. 117.

Levitus, S., Burgett, R., Boyer, T., 1994. World Ocean Atlas 1994, Vol. 3: Salinity. NOAA Atlas NESDIS 3, U.S. Gov. Printing Office, Wash. D.C., pp. 99.

Liss, P.S., Merlivat, L., 1986. Air-sea gas exchange rates: Introduction and synthesis. In: Buat-Ménard, P. (Ed.), The Role of Air-Sea Exchange in Geochemical Cycling. D. Reidel, Hingham, Mass., pp. 113-129.

Millero, F.J., Lee, K., Roche, M., 1998. Distribution of alkalinity in the surface waters of the major oceans. Mar. Chem. 60, 111-130.

Reynolds, R.W., Smith, T.M., 1994. Improved Global Sea-Surface Temperature Analyses Using Optimum Interpolation. J. Clim. 7, 929-948.

Signorini, S.R., McClain, C.R., Christian, J.R., 2001a. Modeling biogeochemical-physical interactions and carbon flux in the Sargasso Sea (Bermuda Atlantic Time-series Study site), NASA/TP 209991. NASA Goddard Space Flight Center, Greenbelt, MD, pp. 37.

Signorini, S.R., McClain, C.R., Christian, J.R., Wong, C.S., 2001b. Seasonal and interannual variability of phytoplankton, nutrients, TCO_2, pCO_2, and O_2 in the eastern Subarctic Pacific. J. Geophys. Res. 106, 31,197-131,215.

Takahashi, T., Feely, R.A., Weiss, R.F., Wanninkhof, R.H., Chipman, D.W., Sutherland, S.C., Takahashi, T.T., 1997. Global air-sea flux of CO_2: An estimate based on measurements of sea-air pCO_2 difference. Proc. Natl. Acad. Sci. U. S. A. 94, 8292-8299.

Tans, P.P., Fung, I.Y., Takahashi, T., 1990. Observational Constraints on the Global Atmospheric CO_2 Budget. Science 247, 1431-1438.

Wanninkhof, R., 1992. Relationship between Wind-Speed and Gas-Exchange over the Ocean. J. Geophys. Res.-Oceans 97, 7373-7382.

Wanninkhof, R., McGillis, W.R., 1999. A cubic relationship between air-sea CO_2 exchange and wind speed. Geophys. Res. Lett. 26, 1889-1892.

Weiss, R.F., Price, B.A., 1980. Nitrous oxide solubility in water and seawater. Mar. Chem. 8, 347-359.

Wentz, F.J., 1997. A well-calibrated ocean algorithm for special sensor microwave/imager. J. Geophys. Res.-Oceans 102, 8703-8718.

REPORT DOCUMENTATION PAGE

Form Approved
OMB No. 0704-0188

1. AGENCY USE ONLY *(Leave blank)*	2. REPORT DATE	3. REPORT TYPE AND DATES COVERED
	April 2002	Technical Memorandum

4. TITLE AND SUBTITLE
Sensitivity of Global Sea-Air CO_2 Flux to Gas Transfer Algorithms, Climatological Wind Speeds, and Variability of Sea Surface Temperature and Salinity

5. FUNDING NUMBERS
970

6. AUTHOR(S)
Charles R. McClain and Sergio Signorini

7. PERFORMING ORGANIZATION NAME(S) AND ADDRESS (ES)
Goddard Space Flight Center
Greenbelt, Maryland 20771

8. PEFORMING ORGANIZATION REPORT NUMBER
2002-01624-1

9. SPONSORING / MONITORING AGENCY NAME(S) AND ADDRESS (ES)
National Aeronautics and Space Administration
Washington, DC 20546-0001

10. SPONSORING / MONITORING AGENCY REPORT NUMBER
TM—2002–211604

11. SUPPLEMENTARY NOTES
S. Signorini, SAIC, Beltsville, Maryland.

12a. DISTRIBUTION / AVAILABILITY STATEMENT
Unclassified–Unlimited
Subject Category: 48
Report available from the NASA Center for AeroSpace Information, 7121 Standard Drive, Hanover, MD 21076-1320. (301) 621-0390.

12b. DISTRIBUTION CODE

13. ABSTRACT *(Maximum 200 words)*

Sensitivity analyses of sea-air CO_2 flux to gas transfer algorithms, climatological wind speeds, sea surface temperatures (SST) and salinity (SSS) were conducted for the global oceans and selected regional domains. Large uncertainties in the global sea-air flux estimates are identified due to different gas transfer algorithms, global climatological wind speeds, and seasonal SST and SSS data. The global sea-air flux ranges from -0.57 to -2.27 Gt/yr, depending on the combination of gas transfer algorithms and global climatological wind speeds used. Different combinations of SST and SSS global fields resulted in changes as large as 35% on the oceans global sea-air flux. An error as small as ±0.2 in SSS translates into a ±43% deviation on the mean global CO_2 flux. This result emphasizes the need for highly accurate satellite SSS observations for the development of remote sensing sea-air flux algorithms.

14. SUBJECT TERMS
Global sea-air CO_2 flux, gas transfer, wind speeds, sea surface temperatures, salinity.

15. NUMBER OF PAGES
25

16. PRICE CODE

17. SECURITY CLASSIFICATION OF REPORT	18. SECURITY CLASSIFICATION OF THIS PAGE	19. SECURITY CLASSIFICATION OF ABSTRACT	20. LIMITATION OF ABSTRACT
Unclassified	Unclassified	Unclassified	UL